

# A PILOT STUDY USING DEEP INFRARED IMAGING TO CONSTRAIN THE STAR FORMATION HISTORY OF THE XUV STELLAR POPULATIONS IN NGC 4625

STEPHANIE J. BUSH<sup>1,\*</sup>, ROBERT C. KENNICUTT<sup>2</sup>, M. L. N. ASHBY<sup>1</sup>, BENJAMIN D. JOHNSON<sup>2</sup>, FABIO BRESOLIN<sup>3</sup>, GIOVANNI FAZIO<sup>1</sup>

*Accepted for publication in ApJ*

## ABSTRACT

In a  $\Lambda$ CDM universe, disk galaxies' outer regions are the last to form. Characterizing their contents is critical for understanding the ongoing process of disk formation, but observing outer disk stellar populations is challenging due to their low surface brightness. We present extremely deep  $3.6\ \mu\text{m}$  observations (Spitzer/IRAC) of NGC 4625, a galaxy known for its radially extended ultraviolet-emitting stellar population. We combine the new imaging with archival UV imaging from the *GALEX* mission to derive multi-wavelength radial profiles for NGC 4625 and compare them to stellar populations models. The colors can be explained by the young stellar population that is responsible for the UV emission and indicate that the current star formation rates in the outermost disk are recent. Extended star formation in NGC 4625 may have been initiated by an interaction with neighboring galaxies NGC 4618 and NGC 4625a, supporting speculation that minor interactions are a common trigger for outer disk star formation and late stage disk growth.

*Subject headings:* galaxies: spiral, galaxies: structure, galaxies: evolution, infrared: galaxies

## 1. INTRODUCTION

In a  $\Lambda$ CDM universe, the inner parts of galactic disks are thought to assemble first. The outer parts then form gradually as higher angular momentum material is accreted. N-body simulations of cosmological disk formation demonstrate this “inside out” disk formation, indicating that since  $z \sim 1$  galaxies evolve proportionally in scale length and mass (Brook et al. 2006; Mo et al. 1998).

While observations confirm stellar disk sizes grow at late times (e.g. Trujillo et al. 2006), the mechanism for mass buildup is unclear. Mass buildup in the outer regions of galaxies can be accomplished several ways. Stellar mass can be redistributed throughout a galaxy as it evolves dynamically in isolation. Roškar et al. (2008b) show that secular evolution, particularly resonant scattering of stars by transient spiral arms (Sellwood & Binney 2002; Roškar et al. 2008b), creates sharp changes (break radii) in the stellar profile whose radii increases with stellar age. Over time, secular evolution populates the outer disks with older stars. Galactic winds can redistribute gas mass throughout a galaxy, preferentially driving outflows where star formation rates are high and accretion where star formation rates are low (Davé et al. 2011b,a). The accretion of low-mass satellites can dynamically induce star formation in outer disks and deposit gaseous and stellar mass throughout the disk (Younger et al. 2007). Stars could also be preferentially formed in the outer parts of galaxies at low redshift. Several theoretical studies have shown

that an increase in the specific angular momentum of in-falling gas as a function of redshift can lead to reservoirs of cold gas being deposited in the outer disk at late times which can then form stars (Samland & Gerhard 2003; Roškar et al. 2010; Kereš & Hernquist 2009), predicting primarily young stellar populations in the outer regions of galaxies.

Recent imaging confirms that star formation takes place throughout galaxies' gas disks, including the outer regions (Herbert-Fort et al. 2012; Barnes et al. 2011). Up to 30% of nearby disk galaxies have ultraviolet (UV) emission, indicating stars  $\lesssim 200$  Myrs old, in their optically faint outer regions (Thilker et al. 2007; Zaritsky & Christlein 2007; Lemonias et al. 2011). These galaxies have been termed Extended Ultraviolet (XUV) disks. XUV disks are not limited to disk galaxies with strong spiral structure. Moffett et al. (2012) found approximately a 40% occurrence of XUV disks in a sample of E/S0 galaxies. Searches for star forming clusters in the outer disks of “normal” galaxies, galaxies not classified as XUV disks, indicate that young stellar clusters are common to  $1.3\text{--}1.5\ R_{25}$ <sup>5</sup> in disk galaxies (Herbert-Fort et al. 2012; Barnes et al. 2011). Muñoz-Mateos et al. (2007) calculated specific star formation rate profiles (sSFR) for 161 galaxies and found marginal evidence for a radial increase in star formation activity, especially in more massive galaxies. However, robust conclusions about disk formation require knowing the star formation history of these outer regions.

The most direct way of determining the star formation history of galaxies is to compare their old and young stellar populations. Low levels of star formation over the lifetime of a galaxy can create a population of old stars that has a surface brightness so low as to make it undetectable under typical ground-based observing condi-

Electronic address: sbush@cfa.harvard.edu

<sup>1</sup> Harvard-Smithsonian Center for Astrophysics, 60 Garden St, Cambridge, MA 02143 USA

<sup>2</sup> Institute of Astronomy, University of Cambridge, Madingley Road, Cambridge CB3 0HA UK

<sup>3</sup> Institute for Astronomy, University of Hawaii, 2680 Woodlawn Drive, Honolulu, Hawaii 96822 USA

\* Current Address: Department of Meteorology, University of Reading, Earley Gate, Reading RG6 6BB UK

<sup>5</sup>  $R_{25}$  is the radius of the 25th B band magnitude isophote, and is traditionally regarded as the boundary between inner (stellar dominated) and outer (gas dominated) disks.

tions (Bush et al. 2008, 2010). Despite this challenge, observers have started to characterize outer star forming regions in the UV, visible and infrared (IR). In M 83, a prototypical XUV disk ( $R_{25} = 6.9'$ , Thilker et al. 2005), the properties of resolved Asymptotic Giant Branch (AGB) stars (Davidge 2010) and spectral energy distribution (SED) fitting of the UV and mid-IR properties of UV-selected clumps (Dong et al. 2008) indicate a population of clusters with ages ranging from 200 Myrs to a few Gyrs without an underlying older low surface brightness disk. The mid-IR properties of UV selected clumps in the outer disks of other galaxies have yielded similar ages (Alberts et al. 2011). Deep B and V band imaging of M 101, an asymmetrical XUV disk that dominates a small galaxy cluster, exhibits considerable azimuthal variation in its radial color profiles with some older spiral structures and some younger structures that were likely formed in recent interactions (Mihos et al. 2013).

The star formation histories of outer disks have also been constrained through measurements of their chemical abundances. Four well-known XUV disks have been shown to have discontinuities between their inner and outer disk abundance profiles and an approximately constant abundance profile in the outer disk with values between approximately 0.2 and  $0.33 Z_{\odot}$  (Bresolin et al. 2009; Gil de Paz et al. 2007a; Goddard et al. 2010; Bresolin et al. 2012). While the existing gas can be enriched to this level by constant star formation over a period of a few Gyrs, the low stellar content in the outer disk appears inconsistent with that level of star formation for an extended time. This discrepancy may indicate recent gas accretion or radial gas mixing. Surprising levels of enrichment in outer disks have been discovered in large spirals (Ferguson et al. 1998), gas-rich dwarfs (Werk et al. 2010a,b) and galaxies with disturbed HI distributions (Werk et al. 2011), indicating this may be common.

Here we present deep *Spitzer/Infrared Array Camera* (IRAC) (Fazio et al. 2004b)  $3.6 \mu\text{m}$  observations of NGC 4625. The diffuse  $3.6 \mu\text{m}$  background emission measured by Spitzer is a thousand times lower than ground based K-band background emission, making it advantageous for studies of low surface brightness stellar populations. NGC 4625 is one of two initial prototype XUV disks with asymmetric UV emission to  $4 \times R_{25}$  ( $R_{25} = 47''$ , Gil de Paz et al. 2005). We use  $3.6 \mu\text{m}$  emission to examine how stellar light varies throughout the disk and look for signs of a low surface brightness infrared disk underlying the UV features. Previous studies of outer disks in the infrared have only been sensitive to the high surface brightness counterparts of UV clumps. We derive  $3.6 \mu\text{m}$  profiles (Section 3) and compare the profile colors to stellar populations models to constrain the star formation history of the outer disk of the galaxy (Section 4.1). We then speculate about how these star formation histories contribute to our understanding of galaxy formation theory.

## 2. OBSERVATIONS AND DATA REDUCTION

### 2.1. NGC 4625

NGC 4625 ( $D = 9.5 \text{ Mpc}$  for  $H_0 = 70 \text{ km s}^{-1} \text{ Mpc}^{-1}$ , Kennicutt et al. (2003)) is a Magellanic dwarf spiral that could be interacting with the neighboring

Magellanic dwarf NGC 4618<sup>6</sup> or the newly discovered dwarf galaxy NGC 4625A (Gil de Paz et al. 2005). The high surface brightness inner disk is of one-armed spiral morphology and is only a few kiloparsecs ( $R_{25} = 1.1' \times 0.95'$ , Kennicutt et al. (2003)) in diameter. It has a well mapped H I disk, coincident with the XUV emission, of nearly constant surface density from its optical radius to  $\sim 5'$  (Bush & Wilcots 2004; Gil de Paz et al. 2005; Kaczmarek & Wilcots 2012). A known low surface brightness optical disk, coincident with the extended H I, has been imaged in the B and R bands, but without the depth needed for precise color measurements in the outer disk (Swaters & Balcells 2002; Gil de Paz et al. 2005). Abundances indicate a discontinuity in metallicity at  $R_{25}$  and a nearly constant outer disk abundance of  $\sim 0.2 Z_{\odot}$  (Goddard et al. 2011).

### 2.2. IRAC Observations

IRAC observations of NGC 4625 were carried out during Spitzer Cycle 6 (PID 60072, PI S. Bush) using standard observing parameters. Each pointing within a  $2 \times 3$  position map having  $252''$  spacing was observed with  $30 \times 100\text{s}$  dithered exposures. We selected a cycling dither and a medium dither pattern amplitude. The observations were configured so that NGC 4625 was centered in the coverage map at  $3.6 \mu\text{m}$ , the more sensitive of the two operating IRAC detectors. Corresponding images taken at  $4.5 \mu\text{m}$  cover the optical disk, but not the entire field surrounding the galaxy that we used to calculate background emission, consequently we do not use them in our analysis. NGC 4625's companion, NGC 4618, intrudes onto a portion of the images.

The first steps in the IRAC data reduction, using the Basic Calibrated Data (BCD), were carried out by team members at the Center for Astrophysics. All BCD frames not containing the center of NGC 4625 were object-masked and median-stacked according to the array detector orientation; the resulting stacked image was then visually inspected and subtracted from the individual BCDs. This was done to eliminate long-term residual images arising from prior observations of bright sources; it also served to minimize gradients in the celestial backgrounds. Dust contamination can be an issue in the  $3.6 \mu\text{m}$  band (Zibetti & Groves 2011), but in the absence of corresponding images taken at longer wavelength IR images (unavailable in the Spitzer warm mission phase, when these observations were taken) we cannot correct for dust contamination. Since we are primarily concerned with the low metallicity, low density outer regions of the galaxy, we would not expect this to significantly alter our results.

After these preliminaries, the images were combined into two spatially-registered mosaics using IRACproc (Schuster et al. 2006). IRACproc augments the capabilities of the standard IRAC reduction software (MOPEX). The software was configured to automatically flag and reject cosmic ray hits based on pipeline-generated masks together with a  $\sigma$ -clipping algorithm for spatially coincident pixels. IRACproc calculates the spatial derivative of each image and adjusts the clipping algorithm accordingly. Thus, pixels where the derivative is low (in the

<sup>6</sup> Odewahn (1991) estimated a lower distance for NGC 4618 of 6.0 Mpc.

field) are clipped more aggressively than are pixels where the spatial derivative is high (point sources). This avoids downward biasing of point source fluxes in the output mosaics.

After mosaicing, a plane was fit to the binned image to subtract a recognizable diffuse background gradient. After masking the galaxies in the image, the data was binned in  $10 \times 10$  pixel bins. The median of the resulting bins was fit with a linear fit in two dimensions following the procedure proposed by Westra et al. (2010, Appendix A). The details of the background subtraction are discussed in Appendix A.

### 2.3. GALEX Observations

NGC 4625 was imaged by Galaxy Evolution Explorer (GALEX) as a part of the Nearby Galaxies Survey (Gil de Paz et al. 2007b) in the Far-Ultraviolet (FUV) and Near Ultraviolet (NUV) bands with a total exposure time of 3242.2 s. The exposures were processed by the GALEX pipeline (Martin et al. 2005, version 6.0.1) and retrieved from the NASA Mikulski Archive for Space Telescopes<sup>7</sup>.

Background counts in the UV images are very low, usually only a few counts per pixel. Consequently background pixel values follow a Poisson distribution and cannot be approximated by a symmetric, Gaussian distribution for background subtraction. Subtracting the mean of a Poisson distribution does not center it symmetrically around zero, leaving a risk that the noise will bias measurements of the signal. When the signal exceeds the background by many orders of magnitude, the background counts can be safely ignored, but faint outer disk features in these images are often only a few times brighter than the mean background. Consequently, careful background subtraction is needed for our study. We rebinned the UV images into pixels large enough that 99% of the newly defined pixels contained at least 10 counts. The resulting FUV pixels are  $9'' \times 9''$  and the resulting NUV pixels are  $3'' \times 3''$  ( $6 \times 6$  and  $2 \times 2$  original pixels respectively). The resulting pixel distribution is Gaussian and can be background subtracted. From this point on, only the rebinned image is used in this work.

The rebinned images were background subtracted using the same technique we used to subtract the background gradient in §2.2. A wide area surrounding both NGC 4625 and its companion NGC 4618 were masked, the rebinned images were now binned for the purposes of background subtraction, and a surface was fit to the median value of the bins following Westra et al. (2010, Appendix A). The surface was fit iteratively, clipping  $3\sigma$  outliers until the fit converged. The FUV image was divided into  $3 \times 3$  pixel ( $27'' \times 27''$ ) bins and the median of the bins was fit with a plane. The NUV image was divided into  $5 \times 5$  ( $15'' \times 15''$ ) pixel bins and fit with a surface of order two in both  $x$  and  $y$  to remove non-linear, large scale variations in the background. Because the galaxy was masked, there is no danger that we subtracted the galaxy's emission with this fit.

### 2.4. HI maps

HI maps of the NGC 4625 field were derived from observations taken with the Very Large Array (VLA) in B and C configurations (Kaczmarek & Wilcots 2012). The moment map was created with natural weighting and 1800 cleaning iterations on the image file. A flux cut off of  $2\sigma$  ( $0.73 \text{ M}_\odot/\text{pc}^2$ ) was applied. The final synthesized beam was  $13.14'' \times 13.02''$ .

## 3. RESULTS

The  $3.6 \mu\text{m}$  and NUV images of NGC 4625 are shown in Figure 1. The filamentary NUV emission extending off the inner disk of the galaxy is the extended ultraviolet disk. At  $3.6 \mu\text{m}$ , a smooth halo of emission surrounds the galaxy. Distant galaxies are abundant and appear as sources across the field. These are difficult to distinguish from any possible clumpy infrared counterparts to the NUV emission. Also present in the image are a few foreground stars, distinguished by the six-pointed IRAC point response function (PRF). Finally, NGC 4625A, a low surface brightness galaxy identified by Gil de Paz et al. (2005), is present to the east of the lower edge of the galaxy.

### 3.1. $3.6 \mu\text{m}$ Profile

To calculate the radial profile of NGC 4625, we had to determine which, if any, of the sources spread across the image are a part of NGC 4625 and which are background galaxies. While in most galaxies  $3.6 \mu\text{m}$  light is dominated by blackbody emission from older stellar populations, stars of all ages emit at  $3.6 \mu\text{m}$  and younger AGB stars can be brighter in the  $3.6 \mu\text{m}$  than older red giant stars. In environments possibly dominated by younger stellar clusters, such as the outer disks, the  $3.6 \mu\text{m}$  emission could be dominated by AGB stars and it is possible that some of the sources in the image are hot young clusters. However, many of them must be high redshift galaxies (Fazio et al. 2004a; Ashby et al. 2013).

Due to the low resolution of the UV data (rebinned image, see § 2) it is very difficult to identify  $3.6 \mu\text{m}$  counterparts to UV clumps. Consequently, we could not separate young stellar clusters from high redshift galaxies based only on FUV, NUV and  $3.6 \mu\text{m}$  emission. Optical imaging is not available to the depth of the  $3.6 \mu\text{m}$  data, which means we could not use the optical colors to discriminate between background galaxies and NGC 4625 sources. It is consequently difficult to assess the contribution these sources have to the overall profile. Given the prevalence of background galaxies in the  $3.6 \mu\text{m}$  (Fazio et al. 2004a; Ashby et al. 2013) and the lack of data to individually assess sources, we chose to mask all sources in the image and analyze only the smooth, unresolved profile of the galaxy. However, we note that we are likely masking a few sources that are a part of NGC 4625 and consequently our derived profile is a lower limit to the total  $3.6 \mu\text{m}$  light.

We used the Astronomical Point source Extractor for MOPEX (APEX) to detect and mask sources. APEX subtracts a local median in  $15 \times 15$  pixel windows from the image to remove any smooth variations in the image, including the unresolved emission from the galaxy, and selects groups of four pixels or more that are  $3\sigma$  above the local noise value. Because the many background galaxies detected by IRAC are not point sources, we did not attempt to fit and subtract every source. Instead,

<sup>7</sup> <http://galex.stsci.edu/GR4/?page=tilelist&survey=allsurveys>

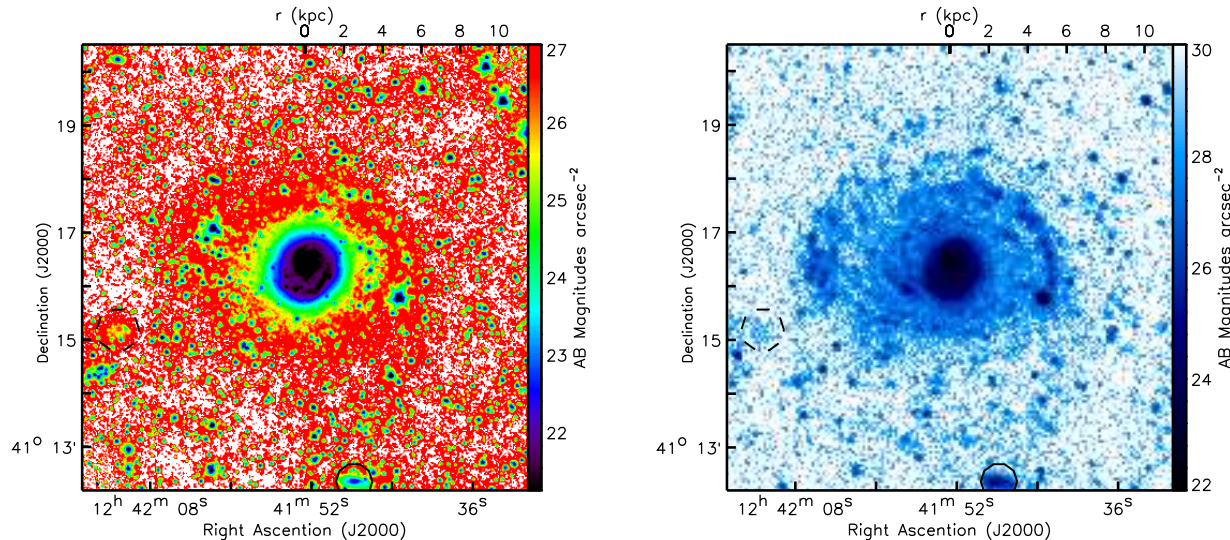


FIG. 1.— Deep Spitzer/IRAC  $3.6\ \mu\text{m}$  image (left) and GALEX NUV image of NGC 4625 (right). North is up and east is to the left. Two galaxies also present in the  $3.6\ \mu\text{m}$  image are circled in black: NGC 4625A (dashed) and SDSS J124147.77 +411222.2 (solid). NGC 4624A is not visible in the NUV.

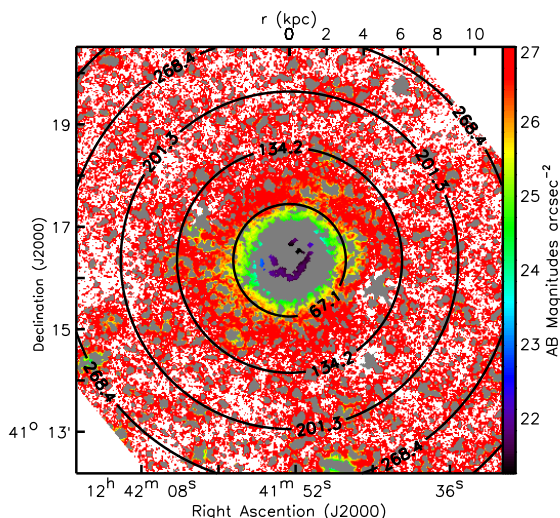


FIG. 2.— Masking of sources in the  $3.6\ \mu\text{m}$  image. Grey areas are masked and the color scale is identical to Figure 1. The higher surface brightness peaks in Figure 1 have been masked using APEX. The remaining emission is used to measure the “unresolved” profile of outer disk light in Section 3.1. Black circles mark radii with arcsecond labels. When doing aperture photometry, five apertures fit between each circle marked here.

all detected sources were masked at  $3\sigma$  above the background noise. To be sure we were accurately accounting for the emission in the wings of true point sources we fitted point response functions (PRFs) by eye to sources obviously exhibiting diffraction spikes and subtracted the fitted PRFs from the image in addition to masking their cores. The masked image is shown in Figure 2. This mask is inappropriate for measuring the profile of the inner disk, because the high surface brightness center of the galaxy is detected as a source, so we used the profile only to analyze outer disk properties.

Next, we measured the  $3.6\ \mu\text{m}$  profile in circular annuli. Apertures are centered on RA = 12h 41m 52.6s and Dec = +41° 16′ 21.5″ (J2000) and are  $13.5''$  wide in order to encompass the beam of the lowest spatial resolution data

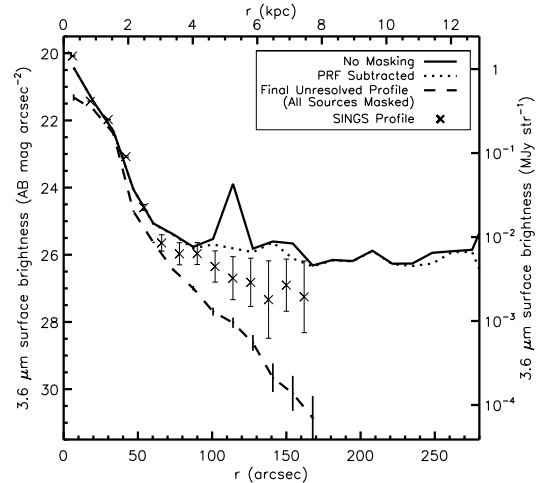


FIG. 3.— The  $3.6\ \mu\text{m}$  profile of NGC 4625 measured with the different masks or lack thereof (images and masks shown in Figures 1 and 2). The solid line is the profile with no masking. The dotted line is the profile with no masking after the PRFs of foreground stars have been subtracted. In these profiles, most of the emission beyond  $70''$  is dominated by background galaxies. The dashed line is the profile after all APEX detected sources are masked. The profiles cease where they fall to the noise level of the background. The  $3.6\ \mu\text{m}$  profile derived from the SINGS survey data by Muñoz-Mateos et al. (2009) is shown as the crosses. For clarity, only every other point is shown. Because SINGS data are only  $1/7$  as deep as our mosaics, the latter is much more sensitive to the halo of unresolved  $3.6\ \mu\text{m}$  emission surrounding the galaxy, which is reflected in smaller error bars. Due to the depth of the data, we also take a different, more conservative, approach to masking background sources than Muñoz-Mateos et al. (2009), which we believe allows us to more accurately characterize the galaxy’s outer disk emission and is primarily responsible for the difference between the two profiles (see § 3.1).

we analyze in this study, the H I maps (§ 2.4). To evaluate the profile error, we chose a distance beyond which we believe all the flux is due to background sources and use apertures beyond that radius to evaluate the error in the background. We chose the radius corresponding to the minimum in the H I profile (13 kpc, derived in Section 3.2) as the edge of the galaxy and use the me-



dian of the flux measured in annuli beyond that radius as the background level. Error bars were derived by taking an estimate of background uncertainty, the standard deviation of the apertures from the median, and adding sampling errors in quadrature. Sampling error is the error associated with having a limited number of pixels to calculate the mean ( $\sqrt{\frac{\sigma}{N}}$  where  $N$  is the number of pixels and  $\sigma$  is the standard deviation of their values).

The profiles are shown in Figure 3. The black solid line is the profile without any masking. Beyond  $75''$ , the profile rapidly flattens because it is dominated by the contribution of background galaxies. The dashed line is the profile with sources masked by APEX. In the outer disk this unresolved emission falls off sharply. We refer to the masked profile as the “unresolved” profile.

Also plotted in Figure 3 is the profile derived from the SINGS survey  $3.6\ \mu\text{m}$  data which is  $1/7$  as deep as our data (Muñoz-Mateos et al. 2009). Muñoz-Mateos et al. (2009) accounted for background galaxies by applying a mask based on IRAC colors. Without deep observations at  $4.5\ \mu\text{m}$  and  $8\ \mu\text{m}$  to compare to our images, this method was not available to us, so we cannot compare the masking methods directly. However, as their study primarily focused on the contents of the inner disk, their masking choice was less conservative than ours and many faint background galaxies remain in their images after masking (Muñoz-Mateos et al. 2009, left side of Figure 2). Consequently we believe our more conservative masking choice allows a better characterization of the profile of the outer disk and that the difference in masking most likely accounts for the difference between the profiles. Our conservative masking choice is inappropriate for the inner disk, so the Muñoz-Mateos et al. (2009) profile should be used to study the inner disk. Note that at the transition between the inner and outer disk, approximately  $60''$ , our profiles agree to within the error bars.

### 3.2. Multi-Wavelength Profiles

To derive colors and gas surface densities, we also calculated FUV, NUV and HI profiles.<sup>8</sup> We first transformed the UV images and HI map to the same pixel scale and orientation as the  $3.6\ \mu\text{m}$  image. The differing resolutions of the  $3.6\ \mu\text{m}$  and UV images make it inappropriate to apply the APEX mask used for the  $3.6\ \mu\text{m}$  image to the UV images. The  $3.6\ \mu\text{m}$  image could be smoothed to the UV resolution prior to masking, but this makes the discrimination between  $3.6\ \mu\text{m}$  sources and the  $3.6\ \mu\text{m}$  smooth emission more difficult. However, the  $3.6\ \mu\text{m}$  bandpass encompasses many more redshifted background galaxies than the FUV and NUV, so background galaxies are not as prevalent in the UV. Consequently, in the UV images, we only masked other low redshift galaxies in the field (NGC 4618, NGC 4625A) and bright foreground stars. Then the profiles were measured with the same apertures as in used for the  $3.6\ \mu\text{m}$  profile (Section 3.1). To subtract the minor contribution from background galaxies, in each band we measured the median surface brightness in point-source masked annuli

<sup>8</sup> The HI profile derived here disagrees with the profile previously derived from the same data by Kaczmarek & Wilcots (2012). After a detailed discussion with the authors, they determined that the profile in Kaczmarek & Wilcots (2012) is too high by a factor of two and an erratum is in preparation. The profile derived here is correct.

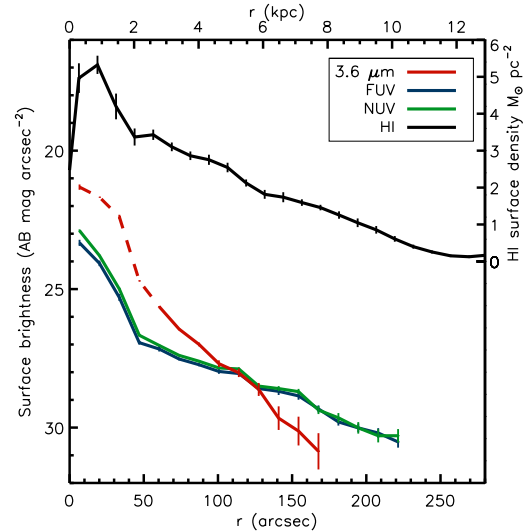


FIG. 4.— Final multi-wavelength profiles after all processing discussed in Section 3.2: HI (black),  $3.6\ \mu\text{m}$  (red), FUV (blue) and NUV (green). The profiles cease when they reach the level of the background noise. The  $3.6\ \mu\text{m}$  profile is dashed where our masking strategy starts to mask the inner disk’s emission. All future figures ignore this region. The  $3.6\ \mu\text{m}$  profile is only for the smooth component of the  $3.6\ \mu\text{m}$  disk.

beyond  $280''$ , and subtracted the median value of these annuli from all aperture values to give the final profiles shown in Figure 4. The error in the profiles is taken to be the standard deviation from this median added in quadrature to aperture sampling errors. The FUV and NUV profiles are consistent with the previous analysis by Gil de Paz et al. (2005), with an inner disk, a break, and a shallower decline in the outer disk. The HI profile shows a slow decline from the break around  $50''$  to  $280''$ . Because the HI distributions of NGC 4625 and its neighboring galaxy, NGC 4618, overlap, the profile then begins increasing again at  $280''$ . For our purposes, we defined the minimum in the HI profile as the edge of NGC 4625.

The  $3.6\ \mu\text{m}$  profile is similar to the UV and HI profiles in that it shows a strong break at  $60''$  and a smoothly declining outer disk.<sup>9</sup> However, the slope of the outer disk profile is much steeper than either the UV or HI outer disk slopes. To quantitatively compare the profiles, we show color profiles in Figure 5. While the FUV–NUV color is constant with radius, the FUV– $3.6\ \mu\text{m}$  color profile drops steeply from edge of the inner disk until it is no longer detected. For comparison we plot the gas phase metallicity gradient measured by Goddard et al. (2011), which, like the multi-wavelength profiles, shows a break at the edge of the inner disk.

## 4. ANALYSIS AND DISCUSSION

### 4.1. Comparison to Stellar Populations Models

To constrain the star formation history of the outer disk of NGC 4625, we compared the derived colors to stellar population models. These models predict the emission of a stellar population with a given star formation

<sup>9</sup> The  $3.6\ \mu\text{m}$  profile in the inner disk is unreliable due to the masking, as higher surface brightness features are masked. If the mask were removed from the inner disk, the break would be stronger. This can be verified by other published profiles of NGC 4625’s inner disk (Muñoz-Mateos et al. 2009).

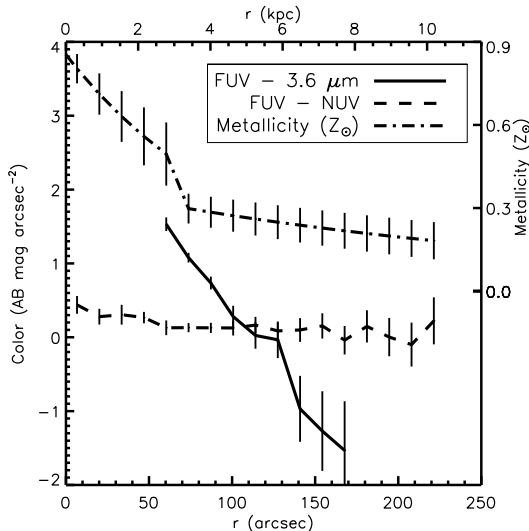


FIG. 5.— FUV–3.6  $\mu\text{m}$  (solid) and FUV–NUV (dashed) color profiles. They are each bluer at larger radii. The FUV–3.6  $\mu\text{m}$  colors correspond to reasonable age ranges in multiple SFH models, shown in Figure 6. The metallicity profile from Goddard et al. (2011) is shown as the dashed-dotted line for comparison.

history, metallicity and initial mass function (IMF). We chose the canonical Bruzual & Charlot (2003) models, which we believe have the most accurate representation of the near-infrared (JHK) contribution of AGB stars. However, we note that the contribution of AGB stars to 3.6  $\mu\text{m}$  emission is not well understood and to estimate the error in the models we also consider Bruzual (2007) models, which differ from Bruzual & Charlot (2003) models by up to a magnitude in the 3.6  $\mu\text{m}$ .

We first compared model colors for two extreme star formation rate histories, a constant star formation rate and an instantaneous burst of star formation (simple stellar population), to our colors. We selected a Chabrier IMF (Chabrier 2003) with mass limits of 0.1 and 100  $M_{\odot}$  and two stellar metallicities based on the gas phase metallicities derived for NGC 4625’s outer disk (Goddard et al. 2011). Using the  $[\text{NII}]/[\text{OII}]$  metallicity indicator calibrated by Bresolin (2007), Goddard et al. (2011) measured that the outer disk abundance ranges from  $0.4 Z_{\odot}$  to  $0.2 Z_{\odot}$ . The comparison is shown in Figure 6, where Bruzual & Charlot (2003) models are the solid lines and Bruzual (2007) models are the dashed lines. Extinction vectors for both a Calzetti et al. (2000) and a Fitzpatrick (1999) Milky Way dust extinction curve for  $E(B - V) = 0.1$  (Gil de Paz et al. 2005) are shown.

#### 4.2. Outer Disk Star Formation History

Figure 6 shows that the FUV – 3.6  $\mu\text{m}$  color provides the stronger constraint on the age of the stellar population and the FUV – NUV color provides the stronger constraint on the star formation history. The FUV–NUV colors, particularly near the edge of the inner disk, are mostly too red to have had a constant star formation history, but towards the edge of the outer disk the FUV–NUV error bars overlap with the constant star formation rate models. Once a star formation history is chosen, the FUV – 3.6  $\mu\text{m}$  color constrains the age. In either case, the declining FUV–3.6  $\mu\text{m}$  color indicates that the age of the outer disk decreases with radius. In

a disk that has undergone a burst, the age of the disk declines with radius from approximately 100 Myr to 10 Myr. In a disk that is constantly star forming, the age declines from approximately 10 Gyrs to 100 Myrs.

Galactic extinction may alter NGC 4625’s colors. The extinction vectors in Figure 6 indicate that observed extinction curves disagree on the amount of extinction in the FUV–NUV, which varies from almost none to 0.2 magnitudes, but they agree fairly well on FUV–3.6  $\mu\text{m}$  extinction of 0.7 to 1.0 magnitudes. Accounting for this extinction, the outer disk colors are more consistent with a single burst of star formation model that has a younger age, but are also more consistent with a constant star formation rate model. It could be argued that applying Calzetti et al. (2000) extinction makes the colors of the inner radii of the outer disk too red to concur with a burst of star formation, but towards the inner disk the population will undoubtedly begin to be a composite of the inner and outer disk stellar populations, making interpretation difficult.

Reddening within NGC 4625 could also alter the colors. Using the  $\text{H}_2$  and  $\text{H I}$  measurements from Schrubba et al. (2011) we made a back-of-the-envelope calculation of the amount of extinction expected using the solar neighborhood value of  $N(\text{H})/E(B - V) = 5.8 \times 10^{21}$  (Bohlin et al. 1978). Depending on the reddening curve used, there could be approximately 0.5 to 0.8  $E(\text{FUV}-3.6)$  at  $60''$  and approximately 0.2 to 0.3  $E(\text{FUV}-3.6)$  at  $170''$ . The maximum difference between  $60''$  and  $170''$  is then 0.5 magnitudes of reddening, which is quite small compared to the 3.5 magnitude drop in color. Consequently, we do not believe the radial gradient in color is due to a radial gradient in extinction.

Existing NUV– $B$  and  $B - R$  color profiles (Gil de Paz et al. 2005) are not precise enough to constrain the star formation history far into the outer disk. Near the edge of the inner disk they agree with the UV and 3.6  $\mu\text{m}$  colors presented here: slightly too red to be constantly star forming and consistent with single stellar populations whose age is loosely constrained between 1 Gyr and 100 Myrs.

While the errors allow for multiple interpretations, taken at face value, the colors of the outer disk imply a stellar population younger than 1 Gyr that decreases in age with radius. In other words, we have not discovered a reservoir of stellar mass that cannot be explained by the young population that is also responsible for the UV emission. However, we have compared the entire FUV profile to the smooth component of the 3.6  $\mu\text{m}$  profile, which may not be a fair comparison. As discussed in § 3.1, without deeper optical data or higher resolution UV data to selectively mask 3.6  $\mu\text{m}$  sources, it is very difficult to determine what portion of the 3.6  $\mu\text{m}$  sources seen near the galaxy are counterparts to young UV clusters. By comparing the colors derived from the unresolved 3.6  $\mu\text{m}$  profile to stellar populations models, we implicitly assumed that no 3.6  $\mu\text{m}$  sources that belong to the galaxy were masked and that the UV and 3.6  $\mu\text{m}$  emission are from the same stellar population. If the 3.6  $\mu\text{m}$  profile is missing some emission due to excessive masking, we would have underestimated the age of the disk.

It is also possible, even likely, that we are detecting a “composite population” of a young outer disk stellar

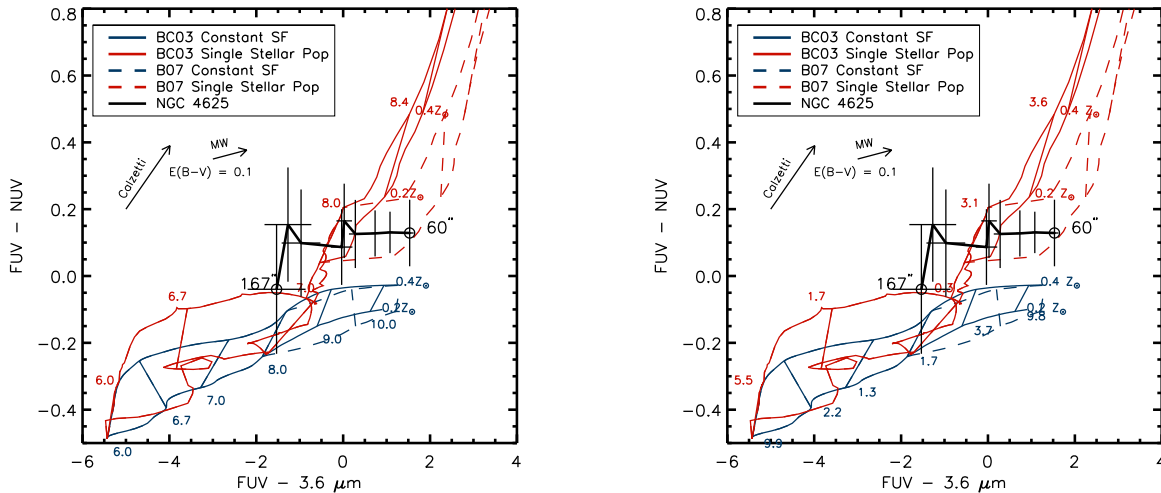


FIG. 6.— The outer disk colors of NGC 4625 (black) compared to Bruzual & Charlot (2003) and Bruzual (2007) stellar populations models with a constant star formation history (blue) and single stellar populations (red). On the left, numbers label  $\log(\text{age})$  in years and metallicity in solar units. On the right, numbers label  $3.6 \mu\text{m}$  mass-to-light ratio and metallicity in solar units. NGC 4625's colors are labeled with their radius in arcseconds. Extinction vectors for Calzetti et al. (2000) and Fitzpatrick (1999) Milky Way dust extinction curves for  $E(B - V) = 0.1$  are shown.

population superimposed on an older, fainter population that extends from the inner disk to the outer disk. This would cause redder colors with decreasing radius as seen in NGC 4625's profiles. Instead of assuming the unresolved  $3.6 \mu\text{m}$  emission and the UV emission are from the same stellar population, we could have assumed that we have masked all the counterparts to the UV emission, because they are not smooth, and that our smooth profile reflects only a different, older population. Of course, the truth is likely in between, but considering both allows us to determine which conclusions are robust to our assumptions.

In Figure 7 we have calculated how long the current star formation rate, derived from the UV profile (Salim et al. 2007), must have been sustained in order to build the mass profile, which is derived from the  $3.6 \mu\text{m}$  emission assuming reasonable  $3.6 \mu\text{m}$  mass to light ratios from Figure 6. In Figure 7, we have also shown how mass to light ratios evolve with age, using stellar populations models with a constant star formation rate until the present and stellar populations models with a constant star formation rate until 200 Myrs ago. The second model is designed to exclude the  $3.6 \mu\text{m}$  contribution from the UV emitting population, which we have now assumed we fully masked. At a given radius, the length of time the disk is required to form stars at the current star formation rate to create the smooth  $3.6 \mu\text{m}$  profile is determined by the age at which the mass-to-light ratio and age are consistent between the two panels of Figure 7. At  $60''$ , using Bruzual & Charlot (2003) models, these are consistent at longer timescales, approximately 8 Gyr with higher mass to light ratios, while at  $170''$ , they are consistent at less than a Gyr, with low mass to light ratios. Of course, if the star formation rate was lower in the past, star formation could have extended further into the past.

While the exact age of the population is difficult to say, two conclusions seem robust to assuming one stellar

population or assuming two independent stellar populations, one emitting in the UV and one emitting in the  $3.6 \mu\text{m}$ . First, the mean age of the outer disk decreases with radius. Second, the star formation at current rates in the outermost disk is a recent event.

While a young outer disk for NGC 4625 certainly seems plausible, there are a few key uncertainties in this analysis. As discussed in § 3.1, Zibetti & Groves (2011) have shown that dust can make a substantial contribution to the  $3.6 \mu\text{m}$  emission, which would violate our assumption that the  $3.6 \mu\text{m}$  emission is emitted by stars. However, it is unlikely that there is enough hot dust in the low density, low metallicity outer disk of NGC 4625 to significantly alter the  $3.6 \mu\text{m}$  emission profile. The stellar populations models also contribute uncertainty. There is easily a factor of two difference in  $3.6 \mu\text{m}$  mass to light ratio between Bruzual & Charlot (2003) and Bruzual (2007), and choice of the initial mass function in these models may significantly alter the predicted emission of younger populations.

It is well established that stars migrate radially from their birthplaces in a galaxy (Roškar et al. 2008b,a) and studies of star formation suggest that at the gas surface densities observed in the outer disk of NGC 4625, star formation occurs with low efficiency (e.g., Martin & Kennicutt 2001). If the stellar content in the outer disk was not born there, our stellar populations analysis does not reflect the characteristics of the outer disk, but rather a scattered inner disk. However, it is unlikely that many stars could migrate as far as 5 kpc from where they were born in less than 150 Myr. Therefore, FUV–NUV colors are unaffected and suggest that NGC 4625's young outer disk was born in-situ, in a low-efficiency sub-threshold regime (Martin & Kennicutt 2001; Kennicutt 1989). However, it is possible that stellar migration from the inner disk has created a low mass older outer disk component coincident with the more recent star formation. Deep optical imaging would fur-

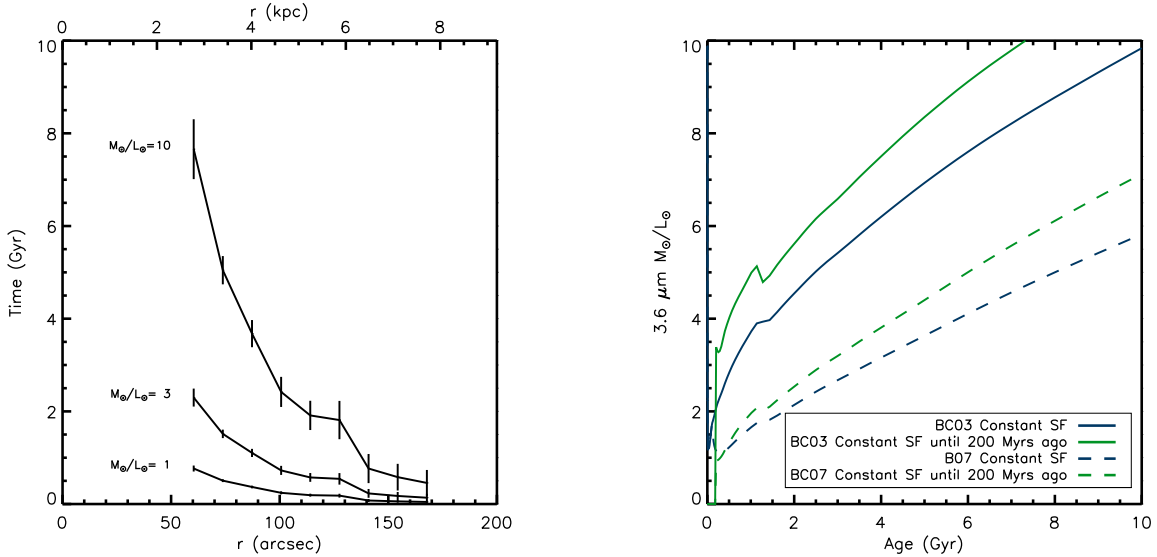


FIG. 7.— Right: The timescale to build up the mass in the outer disk using different 3.6  $\mu\text{m}$  mass-to-light ratios. Left: The 3.6  $\mu\text{m}$  mass to light ratio as a function of age with a constant star formation rate history from Bruzual & Charlot (2003) (solid) and Bruzual (2007) (dashed) stellar populations models. In blue the star formation rate carries on to the present day, in green all star formation ceases 200 Myr ago, approximating the non UV-emitting stellar population.

ther constrain whether the outer disk is a single young population of decreasing age with radius, or a composite population of decreasing average age, but it will not reveal whether this population was born in-situ, or has migrated from the inner disk.

It is difficult to determine conclusively if NGC 4625 is interacting with either of its neighbors: NGC 4618, which is about half its mass (Bush & Wilcots 2004; Kaczmarek & Wilcots 2012) or the dwarf galaxy NGC 4625A. A recent interaction could have compressed gas in the outer disk and initiated star formation in the recent past (Cox et al. 2008; Bush et al. 2008, 2010). The velocity field of the outer HI disk is extremely regular, surprising for a galaxy that has undergone a recent interaction. In fact, parametrized HI morphology of XUV disks galaxies is rarely distinguishable from that of other disk galaxies (Holwerda et al. 2012). However, the star formation rate is very low in the outer disk of NGC 4625 and only a small fraction of the mass needs to be compressed by tidally induced spiral structure to create the UV emission observed (Bush et al. 2008, 2010). If any distortion of the disk by interaction-induced warping is present, it is undetectable in our mosaics, because of the face-on orientation of the galaxy. Several of the best-studied XUV disks show minor signs of interactions, such as extended low surface brightness features, nearby companions or warped outer HI disks, while having an intact inner disk (Chonis et al. 2011; Thilker et al. 2005; Mihos et al. 2013). This suggests the tantalizing possibility that XUV emission is an indication of “flyby” encounters or interactions with a minor perturber.

#### 4.3. The Assembly of the Gaseous Outer Disk and Inside Out Disk Formation

A young NGC 4625 outer disk is consistent with inside-out disk formation and it seems plausible that a recent interaction with a companion caused a burst of star formation in the existing outer gas disk. However, it is still difficult to determine how the extremely extended outer

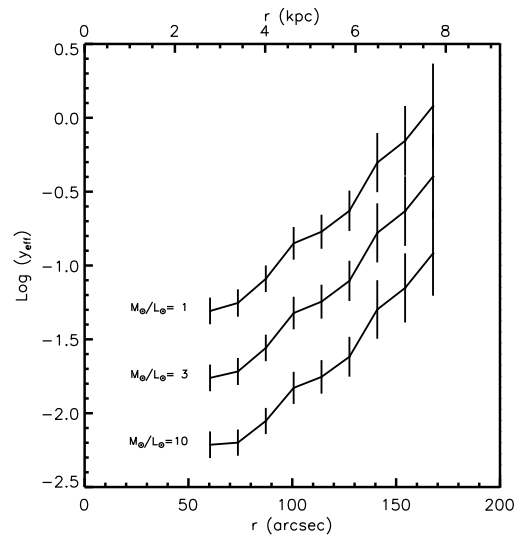


FIG. 8.— The effective metal yield derived from a closed box model and assuming different 3.6  $\mu\text{m}$  mass to light ratios. Error bars represent the errors in the contributing profiles.

gas disk was assembled. The metallicity of the disk gives some clues to its origin. In the closed box chemical evolution model, which assumes a galaxy does not exchange any gas with its environment, the relationship between a galaxy’s gas fraction and metal yield depends only on the mass of stars that have formed in it, and is independent of star formation rate and history. Given a metal yield  $y_{\text{eff}}$ , metal abundance  $Z$  and gas fraction  $\mu$ , under the closed box model  $y_{\text{eff}} = Z/\ln(\mu)$  (Edmunds 1990). We calculate the metal yield required by the closed box model for the gas fraction observed in the outer disk of NGC 4625 assuming HI is the dominant gas mass and a range of 3.6  $\mu\text{m}$  mass to light ratio. The effective metal yield is shown in Figure 8 with error bars reflecting the component profiles’ errors. A reasonable metal yield would imply consistency with a closed box model and suggest that the metal content of the gas is entirely due



to the formation and evolution of the presently observed stellar content. In NGC 4625's outer disk, depending on the mass to light ratio chosen the metal yield increases from around 0.01 at the edge of the inner disk to 0.3 near the edge of the outer disk. These metal yields are very high, consistent with other measurements of outer disk yields (Werk et al. 2011, 2010a) and measured high metallicities in outer disks (Bresolin et al. 2009, 2012) and inconsistent with the closed box model. This suggests that most of the metal content in the outer disk was not created by in-situ star formation.

Bresolin et al. (2012) and Werk et al. (2011) discuss scenarios that could enrich outer disks, including gas accretion and radial metal mixing through either turbulent processes or galactic outflows and re-accretion. They are unable to conclusively determine the mechanism for enriching outer disks and comment that a combination of processes could be at work. In the particular case of NGC 4625, it is plausible that it has exchanged some gas in an interaction with NGC 4618, increasing the size of the outer disk and enriching it while simultaneously initiating star formation. However, it is difficult to explain how a large portion of enriched gas could be exchanged without the corresponding exchange of evolved stars. NGC 4618 also has several large holes in its inner disk HI distribution, indicating past supernovae activity (Kaczmarek & Wilcots 2012). If the two galaxies share a common halo, it is possible supernovae in NGC 4618 have enriched the halo's intergalactic medium. Simulations have also shown that late accretion of halo gas can appreciably increase the gas in an outer disk at late times (Kereš & Hernquist 2009), but this is likely to be extremely low metallicity.

## 5. CONCLUSIONS AND FUTURE DIRECTIONS

We use Spitzer/IRAC to take exceptionally deep  $3.6\ \mu\text{m}$  images of NGC 4625, a prototypical extended ultraviolet disk, to constrain its star formation history and improve our understanding of late stage disk galaxy formation. Since the UV is emitted by stars  $\lesssim 200$  Myrs old and  $3.6\ \mu\text{m}$  emission is emitted by stars of all ages,  $\text{UV} - 3.6\ \mu\text{m}$  color reflects the ratio between recent and past star formation rates and constrains the star formation history of galaxies. We derive the  $\text{FUV} - 3.6\ \mu\text{m}$  and  $\text{FUV} - \text{NUV}$  color profiles of this galaxy. We find that color and luminosity profiles indicate either a decreasing age with radius or that we are observing a composite of distinct stellar populations whose mass varies differently with radius, giving the outer disk a decreasing average age with radius. Our analysis has not revealed a reservoir of stellar mass that cannot be explained by the young population that is also responsible for the UV emission. The decreasing  $3.6\ \mu\text{m}$  luminosity also constrains how long star formation at the current rate could have continued, which is less than 2 Gyr beyond approximately  $1.66\ R_{25}$ . Due to a number of uncertainties, an older, constantly star forming disk at lower star formation rates cannot be ruled out. However, the current star formation rates in the outermost disk are recent.

A young outer disk is consistent with the tenet of  $\Lambda\text{CDM}$  that outer disk formation happens at late times.

Given the presence of companions, it is plausible that star formation was initiated by an interaction a short time ago. The outer disk is metal rich for its stellar content, indicating that gas has been accreted from its environment or could have been exchanged with the companion when star formation was initiated. However, under that scenario, it is not clear why the stars that previously enriched the accreted gas were not also accreted.

Our analysis demonstrates the potential of deep  $3.6\ \mu\text{m}$  imaging of outer disks, but also reveals several key uncertainties. Most importantly, it is difficult to clearly separate the emission from high redshift galaxies along the line of sight from the emission of NGC 4625 itself. Without comparably deep and high resolution optical or UV data, such as Mihos et al. (2013) assembled for M101, we cannot be certain that our  $3.6\ \mu\text{m}$  profile is more than a lower limit on the emission. Additionally, the contribution of dust and AGB star emission to the  $3.6\ \mu\text{m}$  is not well known, complicating the interpretation of existing stellar populations models. Improved theoretical understanding and extremely deep, multi-wavelength datasets of nearby star forming galaxies are required to calculate precise ages of galaxies' farthest reaches. However, these studies are crucial for understanding the evolution of galaxy outskirts and late stage galaxy formation.

## ACKNOWLEDGMENTS

SJB thanks the Institute of Astronomy at the University of Cambridge for welcoming her as a visitor for a year. Special thanks go to Eduard Westra for assistance with background subtraction, Eric Wilcots and Jane Kaczmarek for sharing their HI moment maps and Amanda Kepley for advice on analyzing the HI data. SJB thanks Lars Hernquist and David Thilker for inspiration and countless useful conversations. We also thank an anonymous referee for useful feedback that improved the manuscript. This work is based in part on observations made with the Spitzer Space Telescope, which is operated by the Jet Propulsion Laboratory, California Institute of Technology under a contract with NASA.

## APPENDIX A: BACKGROUND SUBTRACTING THE $3.6\ \mu\text{m}$ IMAGE

Due to the sheer number of sources in this deep IRAC image and the low surface brightness signal we are examining, background subtraction was undertaken very carefully. First, anything that was possibly a source was masked. NGC 4625, its companion NGC 4618 and particularly bright point sources were generously masked by hand, and remaining sources were masked at the  $3\sigma$  level using APEX. Then, the image was binned in  $10 \times 10$  bins, and a plane was fit to the  $3\sigma$  clipped median value of each bin. The binned data was  $2\sigma$  clipped until the fit converged. Figure 9 shows the background subtracted from the image and Figure 10 shows the background subtracted image, with masked areas shown in gray and "X"s over the rejected bins. The two large gray squares mask the galaxies, and the large gray column to the left masks a strip with several bright point sources. Notice that the remaining pixels show small scatter around a value of  $0\ \text{MJy str}^{-1}$ .

## REFERENCES

- Alberts, S., Calzetti, D., Dong, H., Johnson, L. C., Dale, D. A., Bianchi, L., Chandar, R., Kennicutt, R. C., Meurer, G. R., Regan, M., & Thilker, D. 2011, *ApJ*, 731, 28
- Ashby, M. L. N., Willner, S. P., Fazio, G. G., Huang, J.-S., Arendt, R., Barmby, P., Barro, G., Bell, E. F., Bouwens, R., Cattaneo, A., Croton, D., Davé, R., Dunlop, J. S., Egami, E., Faber, S., Finlator, K., Grogin, N. A., Guhathakurta, P., Hernquist, L., Hora, J. L., Illingworth, G., Kashlinsky, A., Koekemoer, A. M., Koo, D. C., Lebbé, J., Li, Y., Lin, L., Moseley, H., Nandra, K.,

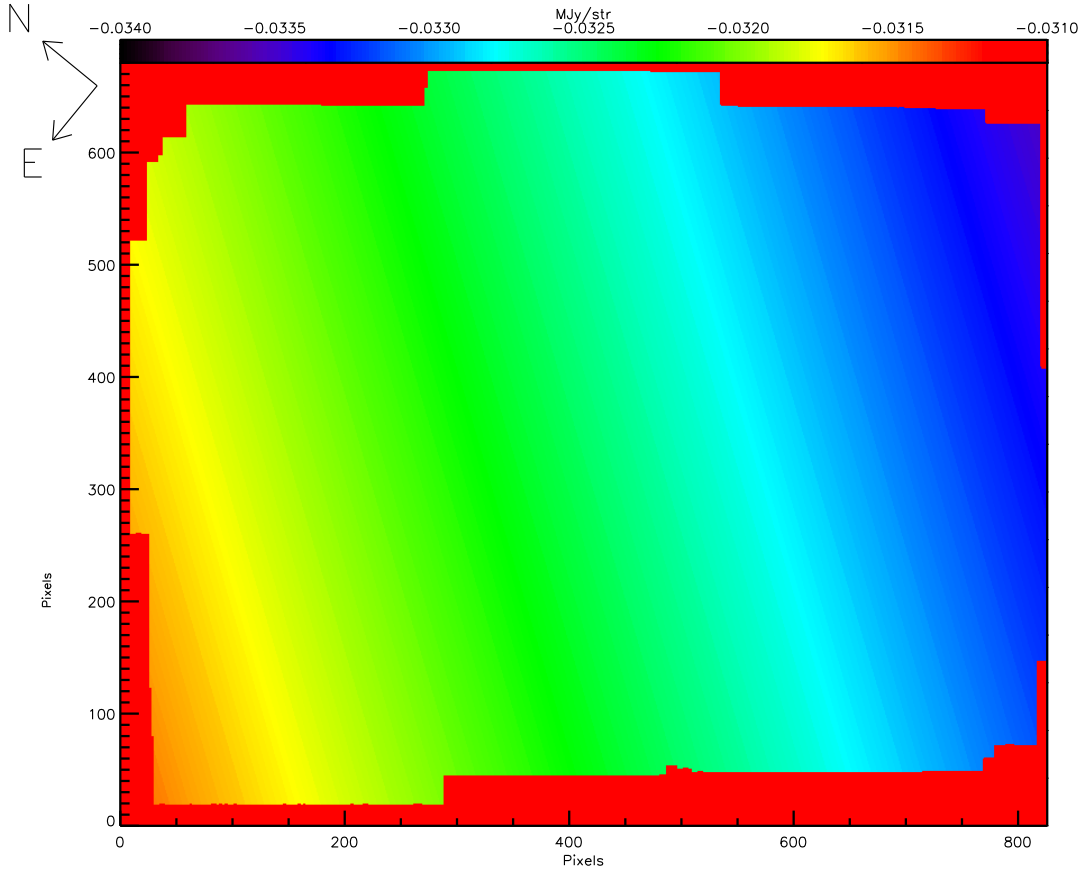


FIG. 9.— The background plane subtracted from the  $3.6\ \mu\text{m}$  image. The axes are in units of pixels, and one pixel equals  $1.22''$  or 56 parsecs.

- Barnes, K. L., van Zee, L., & Skillman, E. D. 2011, *ApJ*, 743, 137
- Bohlin, R. C., Savage, B. D., & Drake, J. F. 1978, *ApJ*, 224, 132
- Bresolin, F. 2007, *ApJ*, 656, 186
- Bresolin, F., Kennicutt, R. C., & Ryan-Weber, E. 2012, *ApJ*, 750, 122
- Bresolin, F., Ryan-Weber, E., Kennicutt, R. C., & Goddard, Q. 2009, *ApJ*, 695, 580
- Brook, C. B., Kawata, D., Martel, H., Gibson, B. K., & Bailin, J. 2006, *ApJ*, 639, 126
- Bruzual, G. 2007, in *Astronomical Society of the Pacific Conference Series*, Vol. 374, *From Stars to Galaxies: Building the Pieces to Build Up the Universe*, ed. A. Vallenari, R. Tantaló, L. Portinari, & A. Moretti, 303–+
- Bruzual, G. & Charlot, S. 2003, *MNRAS*, 344, 1000
- Bush, S. J., Cox, T. J., Hayward, C. C., Thilker, D., Hernquist, L., & Besla, G. 2010, *ApJ*, 713, 780
- Bush, S. J., Cox, T. J., Hernquist, L., Thilker, D., & Younger, J. D. 2008, *ApJ*, 683, L13
- Bush, S. J. & Wilcots, E. M. 2004, *AJ*, 128, 2789
- Calzetti, D., Armus, L., Bohlin, R. C., Kinney, A. L., Koornneef, J., & Storchi-Bergmann, T. 2000, *ApJ*, 533, 682
- Chabrier, G. 2003, *PASP*, 115, 763
- Chonis, T. S., Martínez-Delgado, D., Gabany, R. J., Majewski, S. R., Hill, G. J., Gralak, R., & Trujillo, I. 2011, *AJ*, 142, 166
- Cox, T. J., Jonsson, P., Somerville, R. S., Primack, J. R., & Dekel, A. 2008, *MNRAS*, 384, 386
- Davé, R., Finlator, K., & Oppenheimer, B. D. 2011a, *MNRAS*, 416, 1354
- Davé, R., Oppenheimer, B. D., & Finlator, K. 2011b, *MNRAS*, 415, 11
- Davidge, T. J. 2010, *ApJ*, 718, 1428
- Dong, H., Calzetti, D., Regan, M., Thilker, D., Bianchi, L., Meurer, G. R., & Walter, F. 2008, *AJ*, 136, 479
- Edmunds, M. G. 1990, *MNRAS*, 246, 678
- Fazio, G. G. et al. 2004a, *ApJS*, 154, 39
- . 2004b, *ApJS*, 154, 10
- Ferguson, A. M. N., Gallagher, J. S., & Wyse, R. F. G. 1998, *AJ*, 116, 673
- Fitzpatrick, E. L. 1999, *PASP*, 111, 63
- Gil de Paz, A. et al. 2005, *ApJ*, 627, L29
- . 2007a, *ApJ*, 661, 115
- . 2007b, *ApJS*, 173, 185
- Goddard, Q. E., Bresolin, F., Kennicutt, R. C., Ryan-Weber, E. V., & Rosales-Ortega, F. F. 2011, *MNRAS*, 412, 1246
- Goddard, Q. E., Kennicutt, R. C., & Ryan-Weber, E. V. 2010, *MNRAS*, 405, 2791
- Herbert-Fort, S., Zaritsky, D., Moustakas, J., Di Paola, A., Pogge, R. W., & Ragazzoni, R. 2012, *ApJ*, 754, 110
- Holwerda, B. W., Pirzkal, N., & Heiner, J. S. 2012, *MNRAS*, 427, 3159
- Kaczmarek, J. F. & Wilcots, E. M. 2012, *AJ*, 144, 67
- Kennicutt, Jr., R. C. 1989, *ApJ*, 344, 685
- Kennicutt, Jr., R. C. et al. 2003, *PASP*, 115, 928
- Kereš, D. & Hernquist, L. 2009, *ApJ*, 700, L1
- Lemonias, J. J., Schiminovich, D., Thilker, D., Wyder, T. K., Martin, D. C., Seibert, M., Treyer, M. A., Bianchi, L., Heckman, T. M., Madore, B. F., & Rich, R. M. 2011, *ApJ*, 733, 74
- Martin, C. L. & Kennicutt, Jr., R. C. 2001, *ApJ*, 555, 301
- Martin, D. C. et al. 2005, *ApJ*, 619, L1
- Mihos, C., Harding, P., Spengler, C., Rudick, C., & Feldmeier, J. 2013, *ApJ*, 762, 1
- Mo, H. J., Mao, S., & White, S. D. M. 1998, *MNRAS*, 295, 319

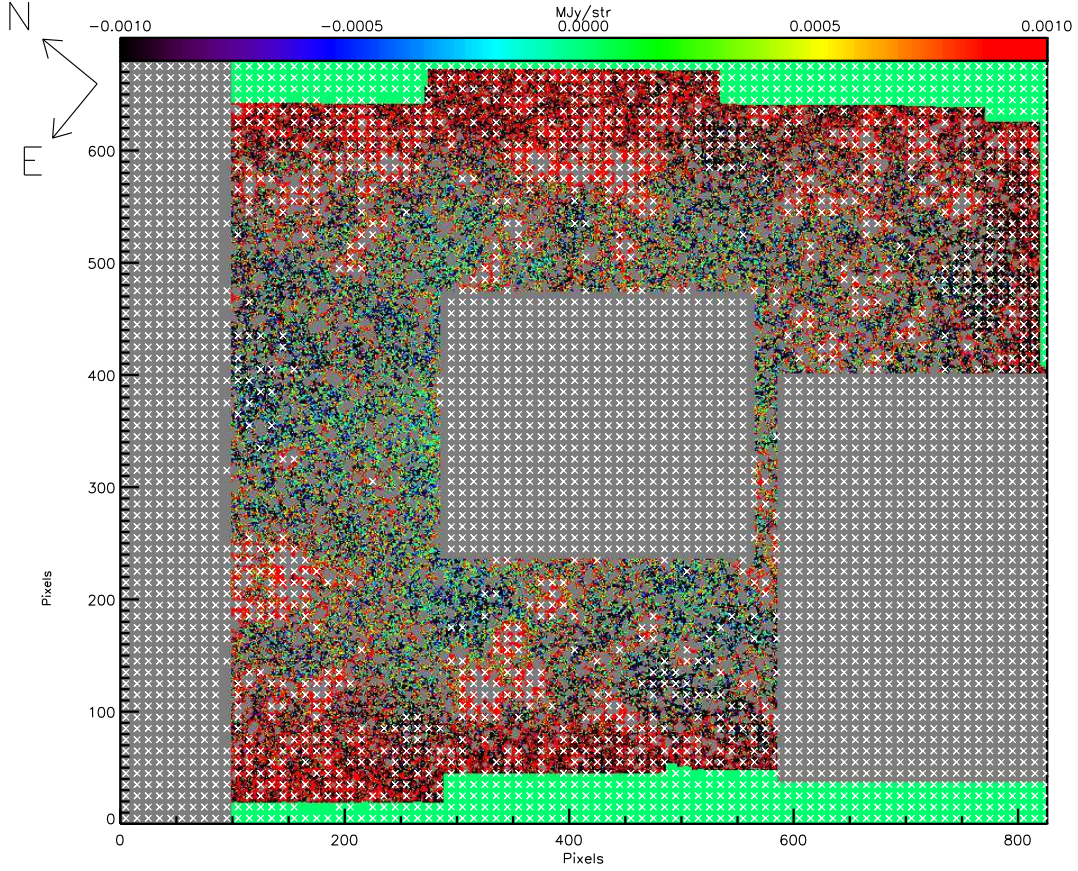


FIG. 10.— The background subtracted  $3.6\ \mu\text{m}$  image. The gray areas are sources that were masked either by hand or using APEX. White crosses show locations that were rejected as outliers from the fit, primarily in masked regions, at the edges of the frame where the exposure time is low due to the dither or around large point sources. Remaining colored points were fit with a plane, and the colors correspond to the post-subtraction emission. The axes are in units of pixels, and one pixel equals  $1.22''$  or 56 parsecs.

- Moffett, A. J., Kannappan, S. J., Baker, A. J., & Laine, S. 2012, *ApJ*, 745, 34
- Muñoz-Mateos, J. C., Gil de Paz, A., Boissier, S., Zamorano, J., Jarrett, T., Gallego, J., & Madore, B. F. 2007, *ApJ*, 658, 1006
- Muñoz-Mateos, J. C. et al. 2009, *ApJ*, 703, 1569
- Odewahn, S. C. 1991, *AJ*, 101, 829
- Roškar, R., Debattista, V. P., Brooks, A. M., Quinn, T. R., Brook, C. B., Governato, F., Dalcanton, J. J., & Wadsley, J. 2010, *MNRAS*, 408, 783
- Roškar, R., Debattista, V. P., Quinn, T. R., Stinson, G. S., & Wadsley, J. 2008a, *ApJ*, 684, L79
- Roškar, R., Debattista, V. P., Stinson, G. S., Quinn, T. R., Kaufmann, T., & Wadsley, J. 2008b, *ApJ*, 675, L65
- Salim, S., Rich, R. M., Charlot, S., Brinchmann, J., Johnson, B. D., Schiminovich, D., Seibert, M., Mallery, R., Heckman, T. M., Forster, K., Friedman, P. G., Martin, D. C., Morrissey, P., Neff, S. G., Small, T., Wyder, T. K., Bianchi, L., Donas, J., Lee, Y.-W., Madore, B. F., Milliard, B., Szalay, A. S., Welsh, B. Y., & Yi, S. K. 2007, *ApJS*, 173, 267
- Samland, M. & Gerhard, O. E. 2003, *A&A*, 399, 961
- Schruba, A., Leroy, A. K., Walter, F., Bigiel, F., Brinks, E., de Blok, W. J. G., Dumas, G., Kramer, C., Rosolowsky, E., Sandstrom, K., Schuster, K., Usero, A., Weiss, A., & Wiesenmeyer, H. 2011, *AJ*, 142, 37
- Schuster, M. T., Marengo, M., & Patten, B. M. 2006, in *Society of Photo-Optical Instrumentation Engineers (SPIE) Conference Series*, Vol. 6270, Society of Photo-Optical Instrumentation Engineers (SPIE) Conference Series
- Sellwood, J. A. & Binney, J. J. 2002, *MNRAS*, 336, 785
- Swaters, R. A. & Balcells, M. 2002, *A&A*, 390, 863
- Thilker, D. A. et al. 2005, *ApJ*, 619, L79
- . 2007, *ApJS*, 173, 538
- Trujillo, I., Förster Schreiber, N. M., Rudnick, G., Barden, M., Franx, M., Rix, H., Caldwell, J. A. R., McIntosh, D. H., Toft, S., Häussler, B., Zirm, A., van Dokkum, P. G., Labbé, I., Moorwood, A., Röttgering, H., van der Wel, A., van der Werf, P., & van Starkenburg, L. 2006, *ApJ*, 650, 18
- Werk, J. K., Putman, M. E., Meurer, G. R., & Santiago-Figueroa, N. 2011, *ApJ*, 735, 71
- Werk, J. K., Putman, M. E., Meurer, G. R., Thilker, D. A., Allen, R. J., Bland-Hawthorn, J., Kravtsov, A., & Freeman, K. 2010a, *ApJ*, 715, 656
- . 2010b, *ApJ*, 715, 656
- Westra, E., Geller, M. J., Kurtz, M. J., Fabricant, D. G., & Dell’Antonio, I. 2010, *PASP*, 122, 1258
- Younger, J. D., Cox, T. J., Seth, A. C., & Hernquist, L. 2007, *ApJ*, 670, 269
- Zaritsky, D. & Christlein, D. 2007, *AJ*, 134, 135
- Zibetti, S. & Groves, B. 2011, *MNRAS*, 417, 812